nature communications



Article

https://doi.org/10.1038/s41467-025-64535-3

Real-space observation of a time-reversal invariant topological state in twisted bilayer InSe

Received: 20 November 2024

Accepted: 19 September 2025

Published online: 27 October 2025

Check for updates

Dacheng Tian^{1,2,8}, Shengdan Tao^{3,4,8}, Yu Wang^{1,2,8}, Peng Cheng ^{1,2}, Yiqi Zhang ^{1,2}, Kehui Wu ^{1,2}, Zeying Zhang⁵, Shengyuan A. Yang⁶, Baojie Feng ^{1,2}, Yunhao Lu ^{3,7} & Lan Chen ^{1,2}

The moiré superlattice formed by van der Waals (vdW) stacking of two-dimensional (2D) monolayers with a twist angle can give rise to a variety of novel correlated physical phenomena. In this study, we propose that a 2D semiconductor composed of vdW layers with band edge states extended into the interlayer region can host time-reversal-invariant topological states, as demonstrated by density functional theory and tight-binding calculations. This emergent physics in moiré superlattices is experimentally verified in a twisted bilayer InSe with a twisting angle of θ = 7.34°. Using scanning tunneling microscopy/spectroscopy (STM/STS), we observed topological edge modes associated with the Z₂ topological metal state at the moiré domain boundary, while these states are absent in the bilayer without twisting. Our theoretical predictions and experimental discoveries advance the field of moiré physics and twistronics, offering a promising strategy for the creation of moiré topological devices.

Recent advances in experimental techniques allowing precise control of twist angles in van der Waals (vdW) layered materials have opened a vast field known as twistronics¹⁻⁷. In these systems, low-energy physics is typically governed by quasiparticles in a moiré superlattice, which can be readily tuned by twisting. The period of this superlattice can be orders of magnitude larger than the lattice constant of the two-dimensional (2D) component layers, leading to surprising emergent physics⁸⁻¹², particularly in terms of electronic correlations^{2,4,5} and topological properties^{7,13,14}. For example, twisted bilayer graphene has been shown to host an unusual electronic structure with "flat bands" at a magic angle of ~1.1°, resulting in strongly correlated electrons and unconventional superconductivity¹⁰. Correlation effects arising from flat bands may also spontaneously break time-reversal symmetry, leading to integer or even fractional quantum anomalous Hall states^{13,14}.

Topological states, however, can exist even in the presence of time-reversal symmetry. Time-reversal-invariant topological insulators in two dimensions, also known as quantum spin Hall insulators, are characterized by a Z_2 topological invariant in the bulk and spin-helical modes at the boundary ^{15,16}. The search for material realizations of such Z_2 topological insulators has been a central focus of research over the past two decades ^{17–24}. Several systems, including semiconductor quantum wells ^{2–5} and 2D materials ^{20,22,25,26}, have been experimentally confirmed. Recently, it has been proposed that the moiré superlattice formed by twisted 2D bilayers MoTe₂ is a versatile platform for realizing time-reversal-invariant topological states ²⁷, which is accomplished experimentally by K. Kang et al ²⁸. Time-reversal invariant (TRI) topological states in twisted 2D semiconductors are also present in twisted bilayer WSe₂. B. A. Foutty et al. provided indirect, yet suggestive evidence for QSH states ²⁹, and the follow-up work from K. Kang

¹Institute of Physics, Chinese Academy of Sciences, Beijing, China. ²School of Physical Sciences, University of Chinese Academy of Sciences, Beijing, China. ³School of Physics, Zhejiang University, Hangzhou, China. ⁴Department of Physics, Shaoxing University, Shaoxing, China. ⁵College of Mathematics and Physics, Beijing University of Chemical Technology, Beijing, China. ⁶Research Laboratory for Quantum Materials, IAPME, Faculty of Science and Technology, University of Macau, Macau SAR, China. ⁷State Key Laboratory of Silicon and Advanced Semiconductor Materials, Zhejiang University, Hangzhou, China. ⁸These authors contributed equally: Dacheng Tian, Shengdan Tao, Yu Wang. ⊠e-mail: bjfeng@iphy.ac.cn; luyh@zju.edu.cn; lchen@iphy.ac.cn

et al made more direct measurements of these states and confirms them via their edge-state conductance³⁰. 2D semiconductors composed of vdW layers with band edge states extending into the interlayer region are particularly promising candidates for enhancing the effects of the moiré superlattice under twisting³¹. Besides, TRI topological states in moiré 2D semiconductors can also be realized in aligned MoTe₂/WSe₂³². But to now, atomic detection in real space of time-reversal-invariant topological states in such twisted vdW semiconductors has remained elusive.

In this work, we investigate the vdW semiconductor InSe as an example, demonstrating that its twisted bilayers generally form a triangular moiré superlattice with an effective p-orbital symmetry. Using first-principles calculations and symmetry analysis, we construct a generic tight-binding (TB) model for these systems. In the presence of spin-orbit coupling (SOC), the bands acquire nontrivial topology. Interestingly, while the band structure exhibits only local gaps, the global gap closes, corresponding to the Z_2 topological metal state proposed in earlier studies²⁹. We experimentally fabricate a twisted bilayer InSe with a twisting angle of θ =7.34°. Scanning tunneling microscopy/spectroscopy (STM/STS) measurements reveal topological edge modes associated with the Z_2 topological metal state at the moiré domain boundary, whereas these states are absent in the bilayer without twisting. Our theoretical and experimental findings pave the way for time-reversal-invariant topological phases and establish

twisted vdW layers as a promising platform for the development of topological devices.

Results and Discussion

Theoretical modeling

InSe is a typical 2D vdW layered material^{33,34}. The structure of a monolayer InSe consists of four atomic sublayers stacked in the order of Se-In-In-Se, each forming a triangular lattice. This structure possesses D_{3h} symmetry (Fig. 1). The calculated band structure for monolayer InSe (Fig. 1a) indicates that InSe is a semiconductor with an almost direct bandgap located around the Γ point. The low-energy bands are predominantly derived from In-s orbitals and Se-p orbitals, with the valence band edge mainly dominated by Se- p_z orbitals (Fig. 1b). Since Se atoms are positioned in the outer sublayer of the InSe monolayer, the states at the valence band edge extend substantially into the interlayer region, making them sensitive to interlayer twisting. This mechanism for moiré physics has been proposed in previous studies²⁷.

Next, we consider a bilayer structure of InSe. Upon twisting, a moiré superlattice is formed, comprising regions with different local stacking configurations, as illustrated in Fig. 1c. The two most distinct configurations are AA and AB stacking. We focus on the two closest Se sublayers in the vdW interlayer region, which are most relevant to our discussion of the valence band edge. In AA stacking, the two Se

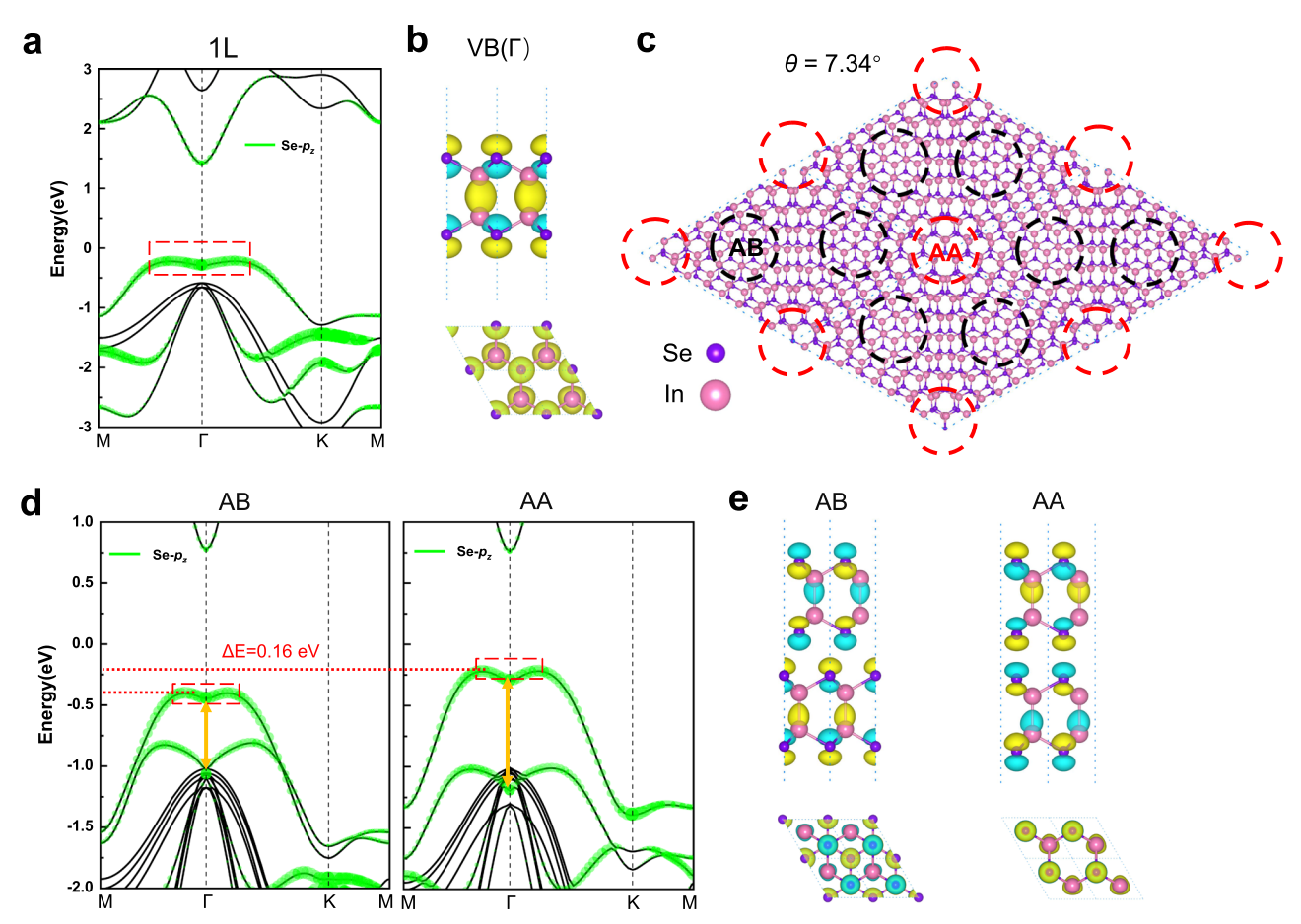


Fig. 1 | **The geometric and band structure of the monolayer and bilayer InSe. a** The band structure of monolayer InSe. The contribution of Se- p_z orbitals is indicated green dots. **b** The side and top view of spatial distribution of wave function of the valence band (VB) edge at $k = \Gamma$, as marked by a red rectangle in **a**. Blue and grey spheres represent In and Se atoms, respectively. Blue and yellow colors represent the phase of wave function. The isosurface value is 3.8×10^{-7} e/bohr³. **c** Twisted bilayer InSe with a twist angle $\theta = 7.34^\circ$. The red and black circles

highlight the AA stacking and AB stacking regions. **d** Energy bands of bilayer InSe with AB stacking and AA stacking configurations. The dash red lines indicate the height of valence band maximum (VBM), and the VBM difference of AA stacking and AB stacking is $\Delta E = 0.16$ eV. The orange double arrows indicate splitting energy for the VBM states in the bilayer of AB stacking and AA stacking are $\Delta E = 0.59$ eV and $\Delta E = 0.89$ eV. **e** The spatial distribution of wave function of the valence bands at $k = \Gamma$, as marked by the red rectangles in **d**.

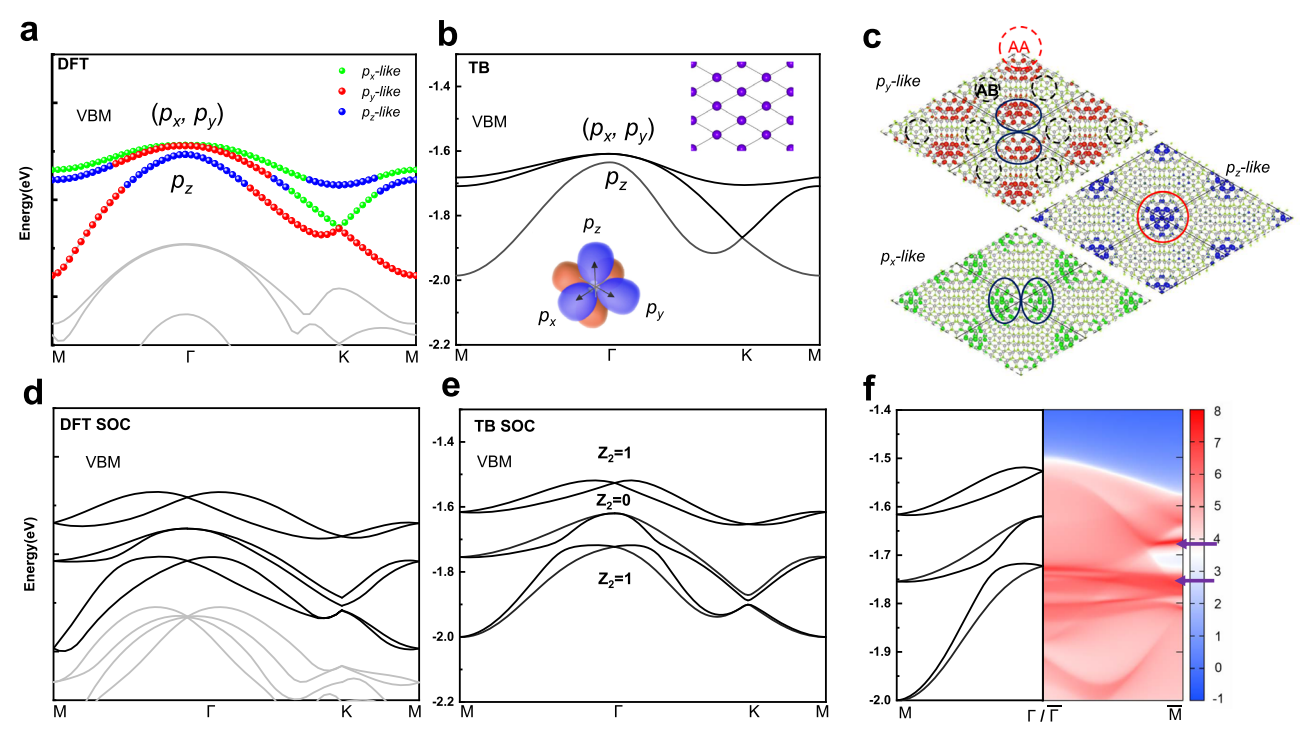


Fig. 2 | **A scenario of the formation of atomic** *p-like* **orbitals. a** Energy bands of twisted 2L InSe with twisted angle θ = 7.34° by density functional theory (DFT) calculations. The topmost three valence bands (VBs) are highlighted by red, green, and blue lines, corresponding to the atomic p_x , p_y and p_z -like orbitals, respectively. The Fermi level is set to zero. **b** Band structure of the (p_x, p_y, p_z) -orbital triangular lattice model with t_1 = -0.285, t_2 = 0.095, t_3 = 0.07, t_4 = -0.04, t_5 = 0.07, t_5 = 0.405 and t_7 = 0.495, where hopping parameters t_1 , t_2 , t_3 , t_4 , t_5 are t_7 are t_7 and t_7 and t_7 are the onsite energies of t_7 and t_7 are the onsite energies of t_7 .

 p_y) and p_z orbitals respectively. The top right and bottom left insets show schematic figures of a triangular lattice and atomic p orbitals, respectively. \mathbf{c} The spatial distribution of wave function for topmost three VBs at Γ , corresponding to the band structure in \mathbf{a} . The isosurface value is 0.00015 e/bohr³. \mathbf{d} , \mathbf{e} Band structure including SOC effect based on the result of \mathbf{a} and \mathbf{b} . $\lambda_I = 0.1$, $\lambda_2 = 0.6$ and $\lambda_p = -0.025$, where λ_1 , λ_2 , λ_p are hopping parameters. \mathbf{f} Comparison between bulk band and edge states, which are indicated by arrows.

sublayers are aligned, meaning their Se atoms are directly above each other. In contrast, in AB stacking, the Se atoms from the upper layer are positioned in the voids of the lower layer. Considering the p_z orbitals on Se sites, which dominate the valence band edge of InSe, it is evident that the two Se sublayers exhibit much stronger interlayer interaction in AA stacking than in AB stacking. This results in a significantly larger splitting of the Se- p_z bands in AA stacking. This expectation is confirmed by density functional theory (DFT) results in Fig. 1d, which compares the band structures for bilayers with AA and AB stacking. A large energy splitting of 0.89 eV is observed at the Γ point for AA stacking, and a smaller splitting of 0.59 eV is found for AB stacking. The valence band maximum (VBM) for AA stacking is $\Delta E \sim 0.16$ eV higher than for AB stacking. Therefore, in the moiré superlattice of bilayer InSe with twisting, which contains both AA and AB stacking regions (Fig. 1c), the AA regions will have the highest VBM energy, surrounded by six minima in AB stacking regions. For holes near the VBM, the AA regions act as potential wells, while the AB regions behave like potential barriers. In other words, the effective physics for holes in this twisted bilayer can be described by a triangular superlattice constructed by the AA regions.

This physical picture is further confirmed by our direct DFT calculations of the twisted bilayers, which include possible lattice reconstruction effects at different twisting angles. We have calculated structures with twisting angles of θ = 32.2°, 21.8°, 13.2°, 9.43°, and 7.34°. These angles were selected based on commensurate structures, satisfying the relation $\cos\theta = \frac{m^2 + 4mn + n^2}{2(m^2 + mn + n^2)}$, where m and n are positive integers. In the following, we focus on the case of θ = 7.34°, as a typical example, while DFT results for other twisting angles are provided in the Supporting Information (SI). The bilayer InSe twisting angle

 θ =7.34° corresponds to the commensurate structure (m, n) = (4, 5), and its moiré supercell contains 488 atoms. Figure 2a shows the calculated band structure for the twisted bilayer in the absence of SOC. We focus on the valence bands. At low energies, three entangled bands are present: the top two are degenerate at the Γ point, while the lower two linearly cross at the K point. The wave function distribution for the three topmost valence band states at the Γ point is plotted in Fig. 2c, indicating that these states are indeed concentrated around AA regions, which correspond to the lattice sites of the triangular superlattice. Interestingly, we find that at each site, these states exhibit p-orbital-like symmetries. The top two states resemble p_x and p_y orbitals at each site, while the lower one is p_z -like. Note that these are not microscopic atomic orbitals, but rather correspond to the moiré superlattice at a much larger scale, representing an emergent physical property.

This key observation suggests that the low-energy physics of the valence band can be described by a triangular lattice model with three p-orbital bases at each site. The twisted bilayer structure breaks the horizontal mirror symmetry of the monolayer, but still approximately respects D_3 symmetry. Constrained by this symmetry, we derive the following TB model on the triangular lattice:

$$H = \begin{bmatrix} \mathscr{E}_{xy} & 0 & 0 \\ 0 & \mathscr{E}_{xy} & 0 \\ 0 & 0 & \mathscr{E}_{zz} \end{bmatrix} + \begin{bmatrix} E_{xx} & E_{xy} & E_{xz} \\ E_{yx} & E_{yy} & E_{yz} \\ E_{zx} & E_{zy} & E_{zz} \end{bmatrix}$$
(1)

where \mathscr{E}_{xy} and \mathscr{E}_{zz} are the onsite energies of (p_x, p_y) and p_z manifolds, respectively. The nearest-neighboring hopping integrals are written as E_{ij} with $i, j \in \{x, y, z\}$ and the details are shown in SI. The band structure

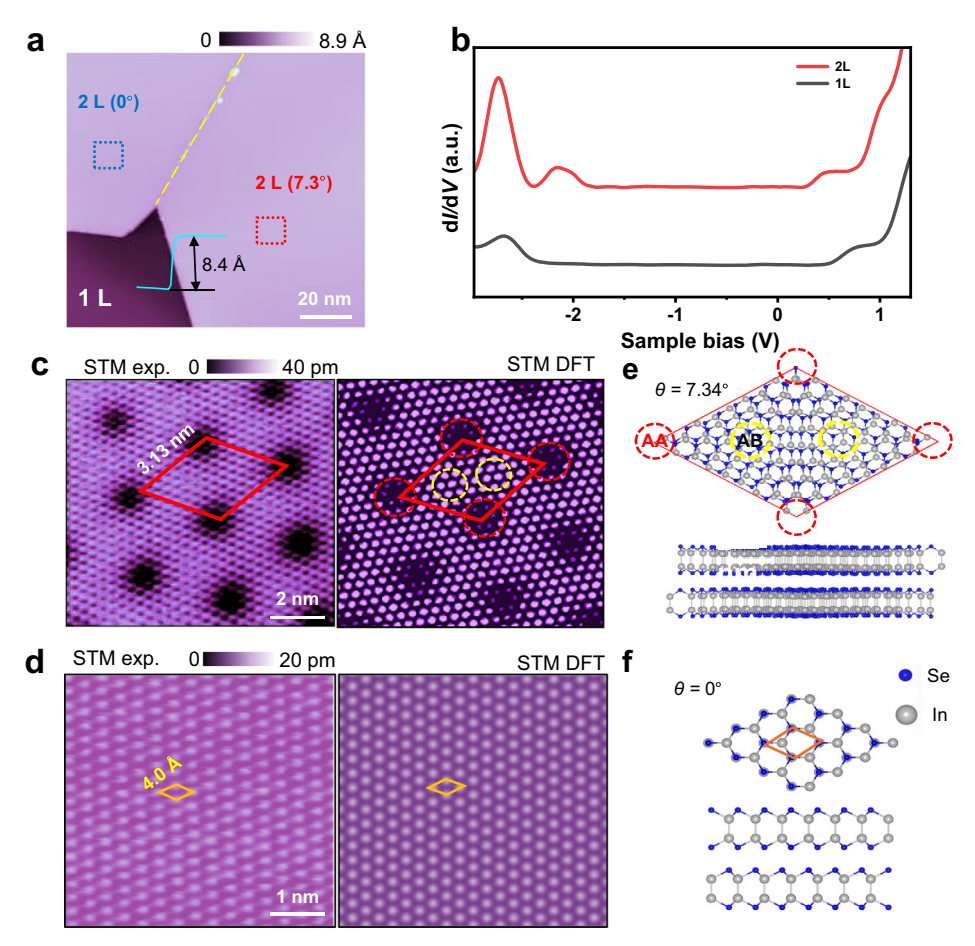


Fig. 3 | **Bilayer InSe on highly oriented pyrolytic graphite (HOPG).** a Large-area scanning tunneling microscopy (STM) image of bilayer InSe on HOPG substrate with two different twisted domains (0° and 7.34°, the dashed line represents the domain boundary) coexisting (with the set bias and current $V_s = 1.5 \text{ V}$, I = 30 pA). **b** The dI/dV curves taken on 1 L and 2 L InSe surfaces. **c**, **d** Left panel: High-resolution experimental STM images of different domains on 2 L InSe surface with twisting angles of 7.34° and 0°, respectively. Each protrusion corresponds to Se

atoms (c: $V_s = -1.1 \text{ V}$, I = 70 pA; d: $V_s = -1.6 \text{ V}$, I = 70 pA). Right panel: Simulated STM images of bilayer InSe with same twisting angle (the red and yellow dashed circles represent AA and AB, respectively). **e**, **f** Top and side view of the atomic structural model of 2 L InSe with twisting angles of 7.34°(single-moiré-unit) and 0°, respectively. Blue and grey spheres represent In and Se atoms, respectively. The moiré supercell is labeled by a red rhombus in **c** and **e** and the 1×1 unit cell is labeled by an orange rhombus in **d** and **f**.

derived from this TB model, shown in Fig. 2b, successfully captures the key features of the DFT results for the twisted bilayer InSe (Fig. 2a), especially the band degeneracies at the Γ and K points.

Including SOC in the DFT calculations lifts the spin degeneracy of each band due to the broken inversion symmetry. As illustrated in Fig. 2d, three pairs of bands appear, and each pair exhibits degeneracy at the Γ point. The top pair of bands is separated from the lower bands by a local direct gap at each k-point in the Brillouin zone, even though the global gap vanishes. In other words, the top pair of bands forms a single band complex, for which the topological properties can be analyzed. In the TB model, we incorporate SOC terms up to first neighbor hopping processes (details are shown in SI). The resulting band structure in Fig. 2e qualitatively agrees with the DFT results (Fig. 2d).

This twisted bilayer InSe system preserves time-reversal symmetry. In 2D, such systems can be characterized by a Z_2 topological invariant. Due to computational complexity, we evaluate this invariant using the TB model results (Fig. 2e). We find that both band complexes—the top two bands and the lower four bands—are topologically nontrivial, resulting in a Z_2 topological metal state³⁵ when the system is hole-doped. The manifestation of this nontrivial topology is the presence of topological edge modes³⁶. Using the TB model, we calculated the edge spectrum, shown in Fig. 2f. The topological edge modes are clearly visible below the top pair of bands. Our calculations indicate

that these modes are located near the edge below the VBM, which will be discussed later.

Experimental results

To demonstrate the existence of twisting-induced topological band structures in bilayer InSe, we performed experimental growth of bilayer InSe and conducted atomic-scale characterization. Bilayer InSe was grown on a highly oriented pyrolytic graphite (HOPG) substrate using molecular beam epitaxy, as shown in the STM image in Fig. 3a. The line profile in the inset shows that the height of the upper layer is approximately 8.4 Å relative to the lower layer, corresponding to the thickness of a monolayer (1L) InSe. In Fig. 3a, the distinct domain boundary in bilayer (2 L) InSe indicates the presence of two naturally formed domains. The differential conductance (dI/dV) spectra of InSe shown in Fig. 3b display stair-like density of states (DOS) in the conduction bands (CBs) and peak-like DOS in the valence bands (VBs), corresponding to 2D electron gas and quantum well states of InSe, respectively, related to the number of layers^{37,38}. As the number of layers increases, the energy position of the first peak gradually approaches the Fermi level, and the bandgap decreases from 2.9 eV for 1L to 2.0 eV for 2 L InSe.

High-resolution STM images of 2L InSe reveal a lattice constant of top-layer Se atoms of 4.0 ± 0.1 Å, consistent with previous studies. However, we identified two types of domains with moiré patterns due

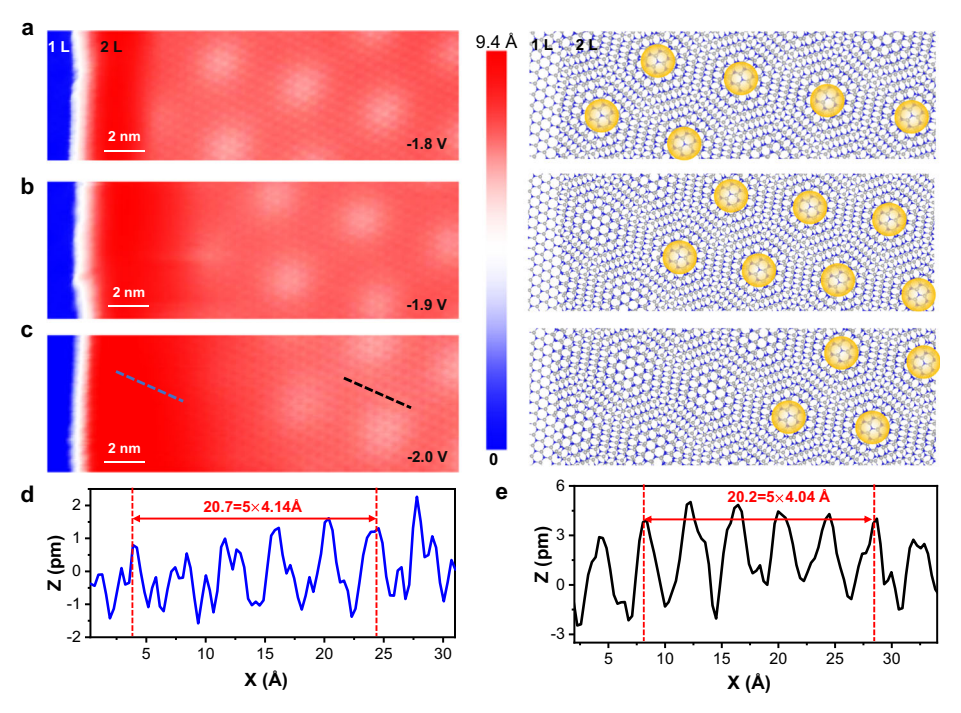


Fig. 4 | **The bias-dependent STM images of twisted bilayer InSe. a–c** High-resolution STM images (left panels) and the corresponding atomic structures (right panels) of bilayer InSe with twisting angle of 7.34° taken at -1.8 V, -1.9 V and -2.0 V.

The yellow circle area represents the AA stacking without breaking the original symmetry. **d** line profile of the region without a moiré pattern along the blue line in **c**. **e** line profile of with a moiré pattern along the black line in **c**.

to different twisting angles between the 1L and 2L InSe, as shown in the left panels of Fig. 3c and 3d. The triangular moiré pattern in Fig. 3c exhibits a lattice period of 3.13 ± 0.05 nm, corresponding to a 7.34° rotation of 2L InSe relative to the underlying 1L InSe. This domain aligns with the bilayer system with a twisting angle of 7.34° calculated in Fig. 2. In contrast, the lattice orientation of the 2 L InSe domain in Fig. 3d is consistent with the underlying 1L InSe, indicating a twisting angle of 0°. The atomic structures of twisted bilayer InSe with $\theta = 7.34^{\circ}$ and 0°, depicted in Fig. 3e and 3f, respectively, show that the moiré lattices closely match the experimental results (details in Methods). For the twisting structure ($\theta = 7.34^{\circ}$), the AA and AB stacking regions are located at the corner and center of the unit cell of the moiré superlattice, respectively, while the non-twisting bilayer ($\theta = 0^{\circ}$) exhibits AB stacking throughout. The corresponding dI/dV curves are shown in Supplementary Fig. 4, which shows the rotated part is nearer to the Fermi level than the unrotated part, and the valence band maximum (VBM) for AA stacking is higher than for AB stacking.

Interestingly, we observed modulation of the moiré pattern by an electric field between the STM tip and the substrate. As shown in the STM images of 2 L InSe with a twisting angle of 7.34° containing a step edge at different bias voltages [Fig. 4a-c], the moiré pattern of 2 L InSe near the step starts to disappear, and the region without a moiré pattern expands as the bias increases from -1.8 V to -2.0 V (The corresponding Fast Fourier Transform is shown in Supplementary Fig. 5). The lattice constant in the region without the moiré pattern is measured to be 4.14 Å, slightly larger than in the region with the moiré pattern (4.04 Å), as shown in Fig. 4d and 4e. The lattice expansion near the edge of 2 L InSe should alter the lattice commensuration between 2 L and 1 L InSe, resulting in the disappearance of the moiré pattern. This lattice expansion by the electric field may be due to dangling bonds at the step edge of semiconductors³⁹. The residual charge from these dangling bonds, along with the electric field between the tip and the sample, can generate a Coulomb force that stretches the surface lattice near the edge of 2 L. This Coulomb force becomes more pronounced as the bias increases, causing the region without a moiré pattern to grow even larger. Additionally, 2D InSe has been reported to exhibit strong piezoelectricity and flexibility^{39–41}, indicating significant ductility and malleability. Our DFT calculations also show that the lattice constant at the edge of an InSe nanoribbon is larger than that in the center (Supplementary Fig. 3).

The disappearance of the moiré pattern induced by the electric field creates two domains in the same terrace of 2L InSe with a continuous lattice. The on-off switching of the moiré pattern in these domains provides an ideal platform for verifying the topological nature of the band structure in twisting bilayer InSe through STS to measure bulk-edge correspondence. Figure 5a-c shows a series of dl/ dV maps taken from the same area of bilayer InSe with a twisting angle of 7.34° containing a step at -2.3 V, -2.0 V, and -1.8 V, respectively. A pronounced electronic state is observed at the domain boundary between the moiré and non-moiré regions at -1.8 V [Fig. 5a], while this edge states disappear at -2.0 V and -2.3 V. In addition, Supplementary Fig. 6, which depicts the spatial spread of the edge states, reveals an exponential decay of the edge state on the terrace side of the step edge. The edge states decay with a characteristic length of $r_0 \approx 0.70$ nm on the crystal side, indicating a strongly confined nature of the edge states42,43.

The edge state at the moiré domain boundary in bilayer InSe with a twisting angle of 7.34° is further confirmed by comparing the experimental DOS at the boundary and terrace with the calculated results. Figure 5d shows the experimental dI/dV curves taken at the domain boundary and terrace of 2 L InSe. A peak is positioned at -2.0 V in the dI/dV curve of the terrace, corresponding to the intrinsic states of bilayer InSe^{37,38}. In contrast, the dI/dV curve taken at the moiré domain boundary reveals a prominent peak at -1.9 V, with an additional shoulder appearing at a lower energy. To better illustrate the extra electronic states, we performed Gaussian fitting on the dI/dV curve taken at the moiré domain boundary [Fig. 5e]. The fitting results reveal three peaks: a major one at -1.90 V, corresponding to the intrinsic states of bilayer InSe, and two smaller ones at -1.75 eV and -1.65 eV, corresponding to the electronic edge states observed in the

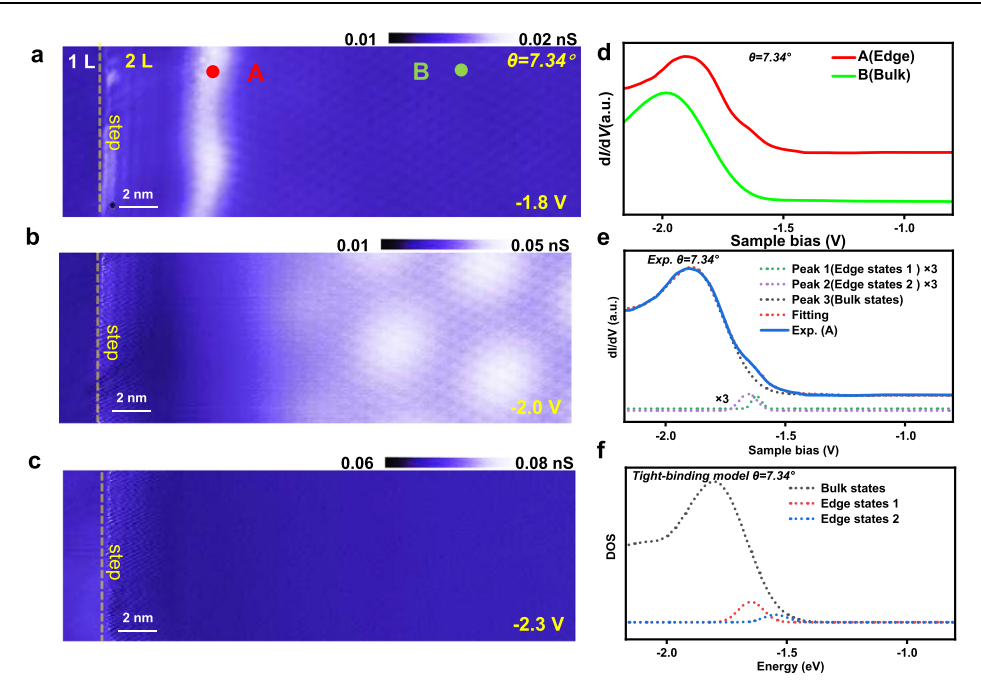


Fig. 5 | **Edge states of bilayer InSe with 7.34° twisting angle.** $a-c \, dl/dV$ maps of bilayer InSe with 7.34° twisting angle (the dashed lines represent the 2 L step). The scanning bias from up to down is $-2.3 \, V$, $-2.0 \, V$ and $-1.8 \, V$ with tunneling current 70 pA. **d** dl/dV curves taken at the Position A and Position B marked in **a** (the

represented curves have been vertically shifted for clarity). **e** Peaks fitting of corresponding d*I*/d*V* curve on Position A in **d**. **f** Calculated density of states (DOS) of bulk and edge states of bilayer InSe with 7.34° twisting angle.

dl/dV map shown in Fig. 5c. Moreover, we calculated the local density of states (LDOS) of bulk and topological edge states in bilayer InSe with a twisting angle of 7.34° using TB theory, as shown in Fig. 5f. The calculated LDOS peak positions are in perfect agreement with the experimental results. Based on the spatial distribution and energy location, the extra electronic states at -1.75 eV and -1.65 eV are identified as topological edge states in twisting bilayer InSe.

To further confirm the topological nature of the band structures in twisted bilayer InSe, we performed STS measurements on a bilayer InSe with a twisting angle of 0° , which did not display any moiré pattern in the STM image [Fig. 3d]. The dl/dV maps of the non-twisted bilayer InSe, including the step edge at various sample biases [Supplementary Fig. 7a], show almost identical features across the entire surface, including the step edge. This observation suggests the absence of edge states in the non-twisted bilayer InSe. Furthermore, the dl/dV curves obtained at the terrace and near the edge of the non-twisted bilayer InSe exhibit a single pronounced peak at -1.90 V, with no additional small peaks or shoulders observed at any other energy range Supplementary Fig. 7c]. By comparing the STS results of the non-twisted bilayer InSe, we infer that the bulk-edge correspondence observed in the moiré domain supports the presence of twisting-induced topological valence bands in the bilayer InSe.

More importantly, we performed STM/STS measurements on $2\,L$ InSe under a magnetic field, as shown in Fig. 6. Figure 6a is a STM image containing the twisted and untwisted parts of $2\,L$ InSe simultaneously. From Fig. 6b, the edge states can be obviously observed at the moiré boundary with $B=0\,T$, where some scratch lines occur in the image, and should result from the moving of a small cluster under the STM tip during scanning. When a small magnetic field was applied, the suppression of edges states occurs. We have repeated these experimental measurements under several magnitude values of magnetic field: $2\,T$, $3\,T$ and opposite $-2\,T$, $-3\,T$, as shown in Fig. 6c-f, and the features are same, suggesting a small magnetic field can break the time-reversal symmetry and suppress the edge states, proving that the edge states are protected by time-reversal symmetry.

Our results demonstrate that twisted bilayer InSe functions as a moiré topological system, characterized by robust edge states. The topological properties are modulated by the twisting angle. These findings, supported by TB and DFT calculations based on a triangular lattice model, identify bilayer InSe as a promising candidate for enhancing our understanding of topological effects in twisted 2D semiconductors and for enabling applications in topological devices, such as flexible topological field-effect transistors⁴⁴⁻⁴⁷.

In summary, we have theoretically proposed an artificial multiorbital triangular lattice in 2D twisted bilayer vdW materials. Using low-temperature STM/STS, we verified the electronic states at the moiré domain boundary in twisted bilayer InSe. Together with DFT calculations, the observed edge states are considered orbital-active topological edge states. Our work reveals a method for generating p-like atomic orbitals in twisted 2D materials. Additionally, we expect that other potential materials, such as GaSe and In_2Se_3 , could also exhibit artificial p orbitals with topological bands close to the Fermi level, paving the way for intriguing avenues of experimental and theoretical exploration of widely tunable topological character.

Methods

DFT methods

Our first-principles calculations were carried out within the density functional theory based on the projected augmented wave (PAW)^{48,49} pseudopotentials as implemented in the Vienna Ab-initio Simulation Package (VASP)⁵⁰. The generalized-gradient approximation (GGA) in the form of Perdew-Burke-Ernzerhof (PBE)⁵¹ functional was used. The cutoff of the plane wave basis was set to guarantee that the absolute energies are converged to a few meV. The DFT-D3 method with Becke-Johnson damping⁵² was employed to incorporate the effects of vdW interactions. The vacuum region was set larger than 15 Å to minimize artificial interactions. Based on the orbital analyses, we constructed the Wannier functions to calculate the topological properties.

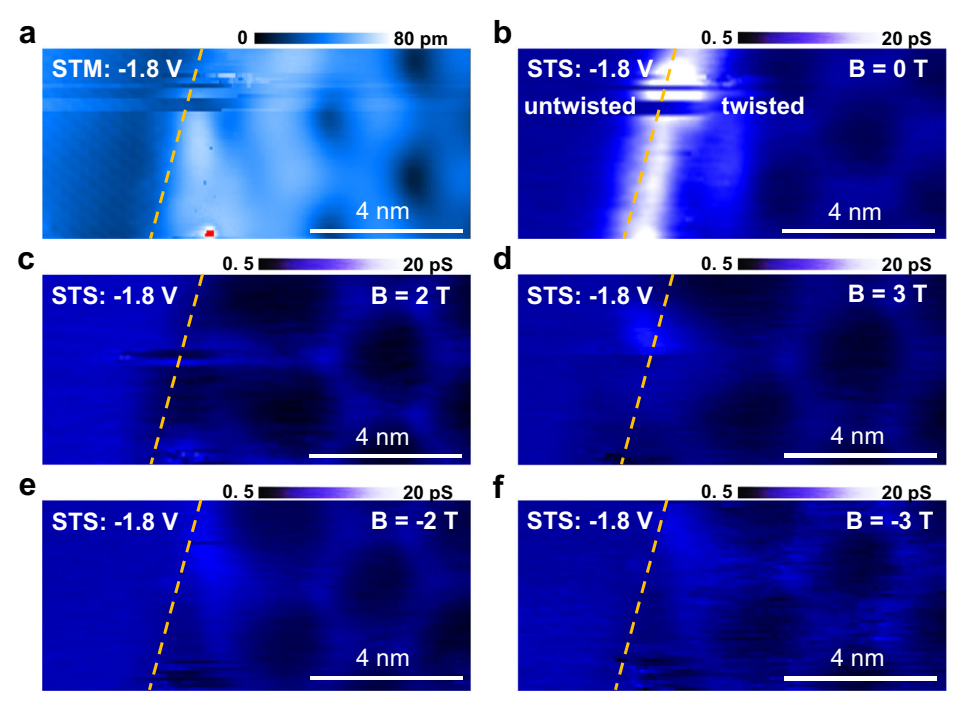


Fig. 6 | **Topological nature of the twisted bilayer InSe. a** STM image bilayer InSe containing the rotated region and unrotated region (dashed line: moiré boundary). **b** Scanning tunneling spectroscopy (STS) mapping acquired at −1.8 V with evident

edge states on the edge of the rotated region (dashed line: moiré boundary). c-f STS mapping acquired at -1.8 V (dashed line: moiré boundary) under a magnetic field of 2 T, 3 T, -2T and -3 T, respectively, with no edge state.

Experimental methods

The bilayer InSe was synthesized by MBE in an ultrahigh vacuum (base vacuum 4×10^{-10} mbar). The HOPG substrate was cleaved and transferred into the UHV chamber to degas at 500 °C. Indium and selenium were simultaneously deposited by two Knudsen cells held at 667 and 126 °C, respectively, and the flux ratio of In: Se is about 1: 2. The temperature of the substrate was kept at 320-350 °C during the InSe growth, to avoid the formation of In₂Se₃ phase. The in situ STM measurements were performed at 77 K on a homemade low-temperature STM interfaced to a Nanonis controller. An electrochemically etched tungsten tip was used for topographic and spectroscopic measurements. We performed in situ STM measurements with an applied outof-plane magnetic field at 4.6 K in the Unisoku STM(1300) system. STM images were taken in the constant current mode, and the voltages refer to the bias on samples with respect to the tip. dI/dV curves were acquired using a lock-in amplifier while the sample bias was modulated by a 667 Hz, 20 mV sinusoidal modulation voltage. STS mapping was obtained for each pixel one after the other under different feedback open/closed, first by scanning and recording the topography of the sample in closed feedback, then by turning off the feedback loop and revisiting these topographic coordinates to measure the differential conductance between the tip and sample. For Grid Spectroscopy, the image was divided into pixels and dI/dV spectra (setpoint: -3.0 V, 70 pA) were obtained at each pixel's location. Finally, a slice of dI/dV at a selected bias for every pixel location was assembled to form another type of STS mapping.

Data availability

Relevant data supporting the key findings of this study are available within the article and the Supplementary Information file. All raw data generated during the current study are available from the corresponding authors upon request

Code availability

The computer code used for numerical calculation and data processing are available from the corresponding authors upon request.

References

- Li, T. et al. Continuous Mott transition in semiconductor moiré superlattices. Nature 597, 350–354 (2021).
- Xu, Y. et al. Correlated insulating states at fractional fillings of moiré superlattices. Nature 587, 214–218 (2020).
- Zhao, W. et al. Emergence of ferromagnetism at the onset of moiré Kondo breakdown. Nat. Phys. 20, 1772–1777 (2024).
- Tang, Y. et al. Simulation of Hubbard model physics in WSe₂/WS₂ moiré superlattices. *Nature* 579, 353–358 (2020).
- Ma, L. et al. Strongly correlated excitonic insulator in atomic double layers. Nature 598, 585–589 (2021).
- Kang, K. et al. Switchable moiré potentials in ferroelectric WTe₂/ WSe₂ superlattices. Nat. Nanotechnol. 18, 861–866 (2023).
- Zeng, Y. et al. Thermodynamic evidence of a fractional Chern insulator in moiré MoTe₂. Nature 622, 69–73 (2023).
- 8. He, F. et al. Moiré patterns in 2D materials: a review. ACS Nano 15, 5944–5958 (2021).
- Wang, L. et al. New generation of Moiré superlattices in doubly aligned hBN/Graphene/hBN Heterostructures. Nano Lett. 19, 2371–2376 (2019).
- Cao, Y. et al. Unconventional superconductivity in magic-angle graphene superlattices. *Nature* 556, 43–50 (2018).
- Zhang, C. et al. Interlayer couplings, Moiré patterns, and 2D electronic superlattices in MoS₂/WSe₂ hetero-bilayers. Sci. Adv. 3, e1601459 (2017).
- 12. Liu, K. et al. Evolution of interlayer coupling in twisted molybdenum disulfide bilayers. *Nat. Commun.* **5**, 4966 (2014).
- Zhang, C. et al. Manipulation of chiral interface states in a moiré quantum anomalous Hall insulator. Nat. Phys. 20, 951–956 (2024).
- Li, T. et al. Quantum anomalous Hall effect from intertwined moiré bands. Nature 600, 641–646 (2021).
- Kane, C. L. & Mele, E. J. Z₂ topological order and the quantum Spin Hall Effect. *Phys. Rev. Lett.* 95, 146802 (2005).
- Bernevig, B. A. & Zhang, S.-C. Quantum Spin Hall Effect. *Phys. Rev. Lett.* 96, 106802 (2006).

- Bernevig, B. A., Hughes, T. L. & Zhang, S.-C. Quantum Spin Hall Effect and topological phase transition in HgTe Quantum Wells. Science 314, 1757–1761 (2006).
- Kane, C. L. & Mele, E. J. Quantum Spin Hall Effect in graphene. *Phys. Rev. Lett.* 95, 226801 (2005).
- Liu, C., Hughes, T. L., Qi, X.-L., Wang, K. & Zhang, S.-C. Quantum Spin Hall Effect in Inverted Type-II Semiconductors. *Phys. Rev. Lett.* 100, 236601 (2008).
- Liu, C.-C., Feng, W. & Yao, Y. Quantum Spin Hall Effect in Silicene and two-dimensional Germanium. Phys. Rev. Lett. 107, 076802 (2011).
- König, M. et al. Quantum Spin Hall insulator state in HgTe Quantum Wells. Science 318, 766–770 (2007).
- Tang, S. et al. Quantum spin Hall state in monolayer 1T'-WTe₂. Nat. Phys. 13, 683–687 (2017).
- Knez, I., Du, R.-R. & Sullivan, G. Evidence for Helical Edge modes in inverted InAs/GaSb Quantum Wells. Phys. Rev. Lett. 107, 136603 (2011).
- Du, L., Knez, I., Sullivan, G. & Du, R.-R. Robust helical edge transport in gated InAs/GaSb bilayers. Phys. Rev. Lett. 114, 096802 (2015).
- 25. Drozdov, I. K. et al. One-dimensional topological edge states of bismuth bilayers. *Nat. Phys.* **10**, 664–669 (2014).
- Yang, F. et al. Spatial and energy distribution of topological edge states in single Bi(111) bilayer. Phys. Rev. Lett. 109, 016801 (2012).
- Wu, F., Lovorn, T., Tutuc, E., Martin, I. & MacDonald, A. H. Topological insulators in twisted transition metal dichalcogenide homobilayers. *Phys. Rev. Lett.* 122, 086402 (2019).
- 28. Kang, K. et al. Evidence of the fractional quantum spin Hall effect in moiré MoTe₂. *Nature* **628**, 522–526 (2024).
- 29. Foutty, B. A. et al. Mapping twist-tuned multiband topology in bilayer WSe₂. Science **384**, 343–347 (2024).
- Kang, K. et al. Double Quantum spin hall phase in Moiré WSe₂. Nano Lett. **24**, 14901–14907 (2024).
- Tao, S. et al. Designing ultra-flat bands in twisted bilayer materials at large twist angles: theory and application to two-dimensional indium selenide. J. Am. Chem. Soc. 144, 3949–3956 (2022).
- 32. Zhao, W. et al. Realization of the Haldane Chern insulator in a moiré lattice. *Nat. Phys.* **20**, 275–280 (2024).
- Kress-Rogers, E., Nicholas, R. J., Portal, J. C. & Chevy, A. Cyclotron resonance studies on bulk and two-dimensional conduction electrons in InSe. Solid State Commun. 44, 379–383 (1982).
- Kuroda, N. & Nishina, Y. Resonance Raman scattering study on exciton and polaron anisotropies in InSe. Solid State Commun. 34, 481–484 (1980).
- Pan, H. et al. Topological metallic phases in spin-orbit coupled bilayer systems. N. J. Phys. 16, 123015 (2014).
- Hasan, M. Z. & Kane, C. L. Colloquium: Topological insulators. Rev. Mod. Phys. 82, 3045–3067 (2010).
- Wang, Y. et al. Nearly ideal two-dimensional electron gas hosted by multiple quantized kronig-penney states observed in few-layer InSe. ACS Nano 16, 13014–13021 (2022).
- 38. Zhang, Z. et al. Strain-induced bandgap enhancement of InSe Ultrathin films with self-formed two-dimensional electron gas. ACS Nano 15, 10700–10709 (2021).
- Zhou, L. et al. Edge engineering in chemically active twodimensional materials. Nano Res. 15, 9890–9905 (2022).
- Sui, F. et al. Sliding ferroelectricity in van der Waals layered γ-InSe semiconductor. Nat. Commun. 14, 36 (2023).
- 41. Wang, X. et al. Probing effective out-of-plane piezoelectricity in van der Waals Layered Materials Induced by Flexoelectricity. Small 15, 1903106 (2019).
- 42. Nayak, A. K. et al. Evidence of topological boundary modes with topological nodal-point superconductivity. *Nat. Phys.* 17, 1413–1419 (2021).
- 43. Litskevich, M. et al. Boundary modes of a charge density wave state in a topological material. *Nat. Phys.* **20**, 1253–1261 (2024).

- 44. Lodge, M. S., Yang, S. A., Mukherjee, S. & Weber, B. Atomically Thin Quantum Spin Hall Insulators. *Adv. Mater.* **33**, 2008029 (2021).
- 45. Molle, A. et al. Buckled two-dimensional Xene sheets. *Nat. Mater.* **16**, 163–169 (2017).
- Qian, X., Liu, J., Fu, L. & Li, J. Quantum spin Hall effect in twodimensional transition metal dichalcogenides. Science 346, 1344–1347 (2014).
- Ren, Y., Qiao, Z. & Niu, Q. Topological phases in two-dimensional materials: a review. Rep. Prog. Phys. 79, 066501 (2016).
- Blöchl, P. E. Projector augmented-wave method. *Phys. Rev. B* 50, 17953–17979 (1994).
- Kresse, G. & Joubert, D. From ultrasoft pseudopotentials to the projector augmented-wave method. *Phys. Rev. B* 59, 1758–1775 (1999).
- 50. Kresse, G. & Furthmüller, J. Efficient iterative schemes for ab initio total-energy calculations using a plane-wave basis set. *Phys. Rev. B* **54**, 11169–11186 (1996).
- Perdew, J. P., Burke, K. & Ernzerhof, M. Generalized gradient approximation made simple. *Phys. Rev. Lett.* 77, 3865–3868 (1996).
- 52. Grimme, S., Ehrlich, S. & Goerigk, L. Effect of the damping function in dispersion corrected density functional theory. *J. Comput. Chem.* **32**, 1456–1465 (2011).

Acknowledgements

We thank the assistance from Ms. Shulin Zhong in the calculation part, and the assistance from Mr. Junming Zhang and Zhongxu Wei in the magnetic field experiments, which were performed in the Synergetic Extreme Condition User Facility (SECUF). This work was supported by the Ministry of Science and Technology (MOST) of China (2024YFA1409100), the National Natural Science Foundation of China (Grant Nos.T2325028, 12134019, 12304239), Guangxi Science and Technology Major Project (Grant Nos: AA23062008-2), and Zhejiang Provincial Natural Science Foundation of China (LDT23F04014F01). L.C. acknowledges the support from the CAS Project for Young Scientists in Basic Research (grant no. YSBR-054), Y.W. acknowledges the support from the Special Research Assistant Program of the Chinese Academy of Sciences, the Postdoctoral Fellowship Program of CPSF (Grant No. GZB20230829), the China Postdoctoral Science Foundation (Grant No. 2023TQ0367).

Author contributions

L.C. and Y.L. proposed and conceived this project. D.T. and Y.W. contributed to the experiment under the supervision of L.C. S.T., S.A.Y. and Y.L. provided the theoretical support for the experiment. D.T., L.C., Z.Z., K.W., P.C., Y.Z. and B.F. did the data analysis. D.T., S.T., Y.W., Y.L. and L.C. wrote the manuscript with the input and comments from all co-authors.

Competing interests

The authors declare no competing interests.

Additional information

Supplementary information The online version contains supplementary material available at https://doi.org/10.1038/s41467-025-64535-3.

Correspondence and requests for materials should be addressed to Baojie Feng, Yunhao Lu or Lan Chen.

Peer review information *Nature Communications* thanks the anonymous reviewers for their contribution to the peer review of this work. A peer review file is available.

Reprints and permissions information is available at http://www.nature.com/reprints

Publisher's note Springer Nature remains neutral with regard to jurisdictional claims in published maps and institutional affiliations.

Open Access This article is licensed under a Creative Commons Attribution-NonCommercial-NoDerivatives 4.0 International License, which permits any non-commercial use, sharing, distribution and reproduction in any medium or format, as long as you give appropriate credit to the original author(s) and the source, provide a link to the Creative Commons licence, and indicate if you modified the licensed material. You do not have permission under this licence to share adapted material derived from this article or parts of it. The images or other third party material in this article are included in the article's Creative Commons licence, unless indicated otherwise in a credit line to the material. If material is not included in the article's Creative Commons licence and your intended use is not permitted by statutory regulation or exceeds the permitted use, you will need to obtain permission directly from the copyright holder. To view a copy of this licence, visit http://creativecommons.org/licenses/by-nc-nd/4.0/.

© The Author(s) 2025